2013

Capacity Fade Model for Spinel $LiMn_2O_4$ Electrode

Yiling Dai
University of South Carolina - Columbia, daiyl880107@gmail.com

Long Cai
University of South Carolina, cailong2005@gmail.com

Ralph E. White
University of South Carolina - Columbia, white@cec.sc.edu

Publication Info

Published in *Journal of the Electrochemical Society*, Volume 160, Issue 1, 2013, pages A182-A190.

Dai, Y., Cai, L., & White, R. E. (2013). Capacity Fade Model for Spinel $LiMn_2O_4$ Electrode. *Journal of The Electrochemical Society*, *160* (1), A182 – A190
Publisher's Version: http://dx.doi.org/10.1149/2.026302jes

Journal of The Electrochemical Society, **160** (1) A182-A190 (2013)
0013-4651/2013/160(1)/A182/9/$28.00 © The Electrochemical Society

Capacity Fade Model for Spinel $LiMn_2O_4$ Electrode

Yiling Dai, Long Cai, and Ralph E White[*,z]

Department of Chemical Engineering, University of South Carolina, Columbia, South Carolina 29208, USA

A mathematical model for the capacity fade of a $LiMn_2O_4$ (LMO) electrode is developed in this paper by including the acid attack on the active material and the solid electrolyte interphase (SEI) film formation on the LMO particle surface. The acid generated by the $LiPF_6$ and the solvent decompositions are coupled to the manganese (Mn) dissolution. The decrease of the Li ion diffusion coefficient is involved as another contribution to the capacity fade, which is caused by the passive film formation on the active material surface. The effects of cell practical operation/fabrication conditions and kinetics of side reactions on battery life are also investigated by utilizing the developed mathematical model.
 [DOI: 10.1149/2.026302jes]

Manuscript submitted August 30, 2012; revised manuscript received November 5, 2012. Published November 26, 2012.

Spinel $LiMn_2O_4$ (LMO) has been considered as one of the most attractive cathode materials for rechargeable lithium-ion batteries because of its low cost, environmentally benign, high cell potential and high rate capability, which especially makes it a favorable candidate for electric vehicles (EV) and hybrid electric vehicles (HEV) application. However, this material exhibits severe capacity fading during cycling or storage at elevated temperature. This shortcoming makes it less competitive with other cathode materials and limits its wide use in commercial batteries.

Several capacity fading mechanisms of spinel electrode have been proposed, such as degradation of the active material, electrolytes decomposition and surface-film formation.[1] Among these, manganese (Mn) dissolution is mainly believed to be the most critical factor resulting in deterioration,[2] although the cause and effect of Mn dissolution is not well understood. Jang et al.[3] proposed that the solvent molecules are electrochemically oxidized and some generated species promote Mn dissolution. They reported that significant amounts of Mn^{2+} ions were detected when a composite electrode was placed near a polarized carbon electrode, but this did not happen when the carbon electrode was left at the open-circuit condition. In their following work,[4] they compared Mn dissolution and capacity loss in Li/LMO cells in various electrolyte solutions. They concluded that acids were generated as a result of electrochemical oxidation of solvent molecules on a composite cathode which caused electrode dissolution. Chromik et al.[5] reported that just after the reversible Li deintercalation a peak of LMO electrode the current rose steeply and a large number of protons were generated in the electrolyte, which were quantitatively measured by using a rotating ring/disk-electrode (RRDE). Also, the solvent irreversible anodic oxidation potential was found to be more negative at the LMO electrode than that at a Pt electrode due to the electrocatalytic activity of LMO. Lee et al.[6] employed the RRDE and a gas analysis technique to study hydrogen evolution in overcharged $LiCoO_2$/graphite cells. Abundance of H_2 evolution during overcharge was observed. They argued that it could not be attributed to the trace water and suggested that the anodic decomposition of the electrolyte was accompanied by acid generation which contributed to the gas evolution. Wang et al.[7] proposed that the acid which is generated in the cell causes Mn dissolution. In addition, solvent oxidation at the cathode and a water reaction with $LiPF_6$ are two main sources of acid generation. Pasquier et al.[8] revealed that generated acid within the cell was responsible for Mn dissolution and formation of a protonated phase. Myung et al.[9] disassembled C/LMO cells cycled at 60°C and found very high HF concentrations in the used electrolyte. An increase of HF concentration was also observed in the electrolyte storage LMO electrode at room and high temperature.[10,11]

Although Mn dissolution was considered to be the critical factor of capacity fading, experimental work found that the capacity losses caused by Mn dissolution alone cannot account for all the capacity fading.[12] Furthermore, factors causing capacity loss may not occur separately. For example, electrolyte oxidation not only causes Mn dissolution but also leads to the loss of cycle lithium. Moreover, the soluble manganese and the produced acid can be transported to anode and be reduced at the anode, which could destroy the solid electrolyte interphase (SEI) film on the carbon anode.[13,14] Also, a passive film was observed on the particle surfaces of the cathode electrode.[15,16] The main sources of film formation come from Mn dissolution which results in inactive material, precipitation of a Mn composite such as MnF_2, as well as the solvent oxidation products.[16,17] This passive film on the cathode active material would block Li ion diffusion into or out of the bulk electrode and lead to cell polarization loss.

Park et al.[18] developed a mathematical model to describe the degradation of spinel LMO cathode based on the mechanism of Mn(III) disproportionation reaction proposed by Lu et al.[19] They argued that the changes in effective transport properties are the important role in capacity degradation. Recently, a more complete model was developed by Cai et al.,[20] which takes the decrease of radius of the active material into account by using a shrinking core model to describe the solid phase diffusion in the cathode. Also, the formation of an inactive material layer which causes a resistance increase in the cathode was included in the model. The kinetics and parameters used in these models were obtained from experiment data where spinel was only statically soaked in the electrolyte. However, it has been reported that the amount of dissolved Mn after cycling or applied potential is much larger than the amount dissolved due to being statically exposed.[3,12]

In this paper, we present an electrochemical model for the capacity fade of the spinel LMO by including acid generation from two side reactions (solvent oxidation on the cathode surface and $LiPF_6$ decomposition) and acid attack induced Mn dissolution. The decrease of the Li ion diffusion coefficient in the solid phase due to the passive film formation on the cathode active material surface was also included as another factor that causes cell capacity loss. The effects of cell operation/fabrication conditions on cell performance were investigated by using the mathematical model presented in this paper. The effects include cell cycling voltage range and the carbon content in the composite electrode. Various kinetic values were chosen to investigate the contribution of the different side reactions to the capacity loss. To exclude the influence of the loss of cycle lithium and the change in the carbon anode, a Li/LMO half-cell was used in the simulations.

Model Development

The model system considered in this paper is a Li/LMO half-cell which consists of a LMO working electrode, a Li metal counter electrode, two layers of 25 μm Celgard separator and 2 M $LiPF_6$ dissolved in EC/DMC/PC. The main side reactions proposed in this model include acid generation from solvent oxidation as well as $LiPF_6$ decomposition, and the acid induced Mn dissolution. These side reactions have been discussed in several experimental reports.[4,7,8,17,21–31] The side reaction scheme and rate expression are presented.

*Electrochemical Society Fellow.
zEmail: white@cec.sc.edu

Side reactions.— It is assumed that the solvent decomposes according to the following oxidation reaction,[4,8,21–23]

$$Solvent \xrightarrow{oxidation} Sl_o + H^+ + e^- \quad [1]$$

where Sl_o represents the overall products of the solvent oxidation and includes soluble species and solid species. The rate of the solvent decomposition is charge-transfer-kinetic controlled and can be expressed by a Butler-Volmer expression as follows:

$$i_s = i_{0,s}\left[\exp\left(\frac{\alpha_{a,s}F}{RT}\eta_s\right) - \exp\left(-\frac{\alpha_{c,s}F}{RT}\eta_s\right)\right] \quad [2]$$

$$\eta_s = \phi_1 - \phi_2 - U_{side} \quad [3]$$

where $i_{0,s}$ is the exchange current density, F is Faraday's constant, R is the universal gas constant, T is the environment temperature, η_s is the over-potential for the electrochemical side reaction in equation 1 and is defined as the difference between the solid phase potential, ϕ_1, and the solution phase potential, ϕ_2, with respect to the equilibrium potential of the side reaction, U_{side}.

An anodic Tafel expression can be used to describe the rate expression if the decomposition reaction is considered to be irreversible. Consequently, the rate expression can be simplified as follows:[24]

$$i_s = i_{0,s}\exp\left(\frac{\alpha_{a,s}F}{RT}\eta_s\right) \quad [4]$$

The H^+ production rate due to the reaction given in equation 1 can be written as follows:

$$R_{s,1} = \frac{i_s}{F} \quad [5]$$

The acidity of the electrolyte containing a $LiPF_6$ salt can be affected by the reaction of $LiPF_6$ with residual water in the organic solvent.[26,32] That is, the $LiPF_6$ salt is decomposed as follows:

$$LiPF_6 \rightarrow LiF + PF_5 \quad [6]$$

where the product PF_5 reacts with water to form HF:

$$PF_5 + H_2O \rightarrow POF_3 + 2HF \quad [7]$$

The reaction rate of $LiPF_6$ decomposition is given by:[27,28]

$$R_{s,2} = k_2[H_2O]^2[LiPF_6] \quad [8]$$

where k_2 is the reaction rate constant for the $LiPF_6$ decomposition reaction, $[LiPF_6]$ is the total $LiPF_6$ concentration added in the electrolyte including ionized $LiPF_6$. The concentration, $[LiPF_6]$, can be approximated by the concentration of Li^+, $[Li^+]$, due to the high ionization of $LiPF_6$. That is:

$$R_{s,2} = k_2 c_{H_2O}^2 c_{Li^+} \quad [9]$$

where c_{H_2O} is concentration of H_2O, $[H_2O]$, c_{Li^+} is concentration of Li^+, $[Li^+]$.

The acid attack on the active material in the cathode, $LiMn_2O_4$, is assumed to occur as follows:[4,7,8,29]

$$4H^+ + 2LiMn_2O_4 = 2Li^+ + Mn^{2+} + \frac{3}{2}Mn_2O_4 + 2H_2O \quad [10]$$

It is supposed that the reaction rate for acid attack on the active material shown in equation 10 is dominated by the acid concentration in the solution.[4,30,31] Consequently, the reaction rate for the reaction in equation 10 is given by:

$$R_{s,3} = k_3 c_{H^+} \quad [11]$$

where k_3 is the reaction rate constant for the acid attack on the active material, c_{H^+} is concentration of H^+, $[H^+]$.

Electrochemical model.— The material balance for Li^+ in the electrolyte is given as follows:

$$\varepsilon_{2,j}\frac{\partial c_{Li^+}}{\partial t} = -\nabla(-D_{eff,Li}\nabla c_{Li^+}) - R_{s,2} + \frac{1-t^+}{F}a_j i_{n,j},\ j = pos, sep \quad [12]$$

where $\varepsilon_{2,j}$ is the porosity of j region (pos = positive, sep = separator), $D_{eff,Li}$ is the effective diffusion coefficient of Li^+ in the binary electrolyte, t^+ is the transference number, a_j is the specific area, $i_{n,j}$ is the local transfer current density in the electrode region j. In the separator region ($j = sep$), the last term in equation 12 is zero since there is no Li intercalation/deintercalation reaction. The specific area in the positive electrode, a_{pos}, is defined as:

$$a_{pos} = 3\frac{\varepsilon_{1,pos}}{R_{pos}} \quad [13]$$

where $\varepsilon_{1,pos}$ is volume fraction of the solid active material in the positive electrode, and R_{pos} is radius of the spherical particle.

The current density distribution in the solid phase, i_1, is given by Ohm's law as follows:

$$i_1 = -\sigma_{eff}\nabla\phi_1 \quad [14]$$

where σ_{eff} is the effective electronic conductivity of the cathode.

The current density in the electrolyte i_2 is given in a modified form of Ohm's law as follows:

$$i_2 = -\kappa_{eff}\left[\nabla\phi_2 - 2\frac{RT(1-t^+)}{F}\nabla\ln c_{Li^+}\right] \quad [15]$$

where κ_{eff} is the effective ionic conductivity of the electrolyte in the cathode.

The total current density is conserved and thus:

$$\nabla\cdot(i_1 + i_2) = 0 \quad [16]$$

Due to conservation of charge, the divergence of the current density in the solution phase can be related to the two electrochemical reactions: Li intercalation/deintercalation reaction and solvent oxidation side reaction as follows:

$$\nabla\cdot i_2 = \sum_{k=1,2} a_k i_{n,k} \quad [17]$$

where a_k represents the specific surface area, $i_{n,k}$ represents the pore wall flux current density of Li intercalation/deintercalation reaction ($k = 1$) and solvent oxidation side reaction ($k = 2$), respectively:

$$\begin{aligned} a_1 &= a_{pos} \\ i_{n,1} &= i_{n,pos} \\ i_{n,2} &= i_s \end{aligned} \quad [18]$$

Guyomard et al.[21] reported that the solvent oxidation occurs mostly on the conductive carbon black, so the area per unit volume for the solvent oxidation, a_2, is related to the carbon content (weight percent), X_c%, in the composite electrode as follows:

$$a_2 = \frac{X_c}{X_{c,set}}a_{2,set} \quad [19]$$

where $X_{c,set}$ represent the carbon content for a preset value and it is set to 10%; $a_{2,set}$ is value of a_2 corresponding to the preset carbon content $X_{c,set}$. The value of $a_{2,set}$ is reported by $a_{2,set}i_{0,s}$ as given in Table II.

Substitution equation 15 into 17 yields,

$$\nabla\cdot\left(\kappa_{eff}\nabla\phi_2 - 2\frac{\kappa_{eff}RT(1-t^+)}{F}\nabla\ln c_{Li^+}\right) = \sum_{k=1,2} a_k i_{n,k} \quad [20]$$

where the source term on the right side of equation 20 is zero in the separator region.

Substitution of equations 14 and 17 into 16 yields:

$$\nabla\cdot(-\sigma_{eff}\nabla\phi_1) = -\sum_{k=1,2} a_k i_{n,k} \quad [21]$$

Because the concentration of salt $LiPF_6$ is much higher than the concentrations of H^+ and Mn^{2+} in the solution, we assume that the fluxes of H^+ and Mn^{2+} in the solution are not affected by the electric field in the solution and their effects on the electric filed are negligible. Therefore, the migration term can be ignored in the material balance for H^+ and Mn^{2+}. The material balance for H^+ in the electrolyte is given by:

$$\varepsilon_{2,j}\frac{\partial c_{H^+}}{\partial t}=\nabla\cdot(D_{eff,H^+}\nabla c_{H^+})+a_2R_{s,1}+2R_{s,2}-4a_jR_{s,3},\ j=pos,sep \quad [22]$$

The material balance for Mn^{2+} in the electrolyte is given by:

$$\varepsilon_{2,j}\frac{\partial c_{Mn^{2+}}}{\partial t}=\nabla\cdot(D_{eff,Mn^{2+}}\nabla c_{Mn^{2+}})+a_jR_{s,3},\ j=pos,sep \quad [23]$$

The material balance for H_2O in the electrolyte is given by:

$$\varepsilon_{2,j}\frac{\partial c_{H_2O}}{\partial t}=\nabla\cdot(D_{eff,H_2O}\nabla c_{H_2O})-R_{s,2}+2a_jR_{s,3},\ j=pos,sep \quad [24]$$

In equations 22-24, a_j and a_2 are zero in the separator region ($j=sep$) because the heterogeneous side reactions do not occur in the separator.

The governing equation for the volume fraction of the active material in the matrix phase which accounts for the acid induced Mn dissolution (side reaction in equation 10) is given by:

$$\frac{\partial\varepsilon_{1,pos}}{\partial t}=-a_{pos}R_{s,3}\overline{V} \quad [25]$$

where $\overline{V}$ is the molar volume of LMO.

It is assumed that the total volume of the solid phase (including active material and inactive material) is not changed due to the side reaction shown in equation 10, that is, the active material degrades to the same volume of the inactive material.

It is assumed that the particles of the active material in the cathode are spheres. The material balance in the particles can be written using Fick's second law as follows:

$$\frac{\partial c_s}{\partial t}=\frac{1}{r^2}\frac{\partial}{\partial r}\left[D_sr^2\left(\frac{\partial c_s}{\partial r}\right)\right] \quad [26]$$

The intercalation/deintercalation kinetics is written in the form of Butler-Volmer equation:

$$i_{n,pos}=i_{0,Li}\left[\exp\left(\frac{\alpha_{a,Li}F}{RT}\eta_{Li}\right)-\exp\left(-\frac{\alpha_{c,Li}F}{RT}\eta_{Li}\right)\right] \quad [27]$$

where η_{Li} is the over potential for Li intercalation/deintercalation reaction, $i_{0,Li}$ is exchange current of Li intercalation/deintercalation reaction, and expressed as:

$$i_{0,Li}=k_{Li}c_{s,surf}^{0.5}(c_{s,\max}-c_{s,surf})^{0.5}c_{Li^+}^{0.5} \quad [28]$$

where k_{Li} is the reaction rate constant in the positive electrode, $c_{s,surf}$ is the surface concentration of Li^+ in the particles in the positive electrode, $c_{s,\max}$ is the maximum concentration of Li^+ in the particles in the positive electrode, and:

$$\eta_{Li}=\phi_1-\phi_2-U_p \quad [29]$$

where U_p is the equilibrium potential of Li intercalation/deintercalation reaction in cathode relative to a lithium reference electrode.

Moreover, the Li ion diffusion coefficient in the solid phase changes due to the plugging of pores and the formation of the film on the LMO particles surface in the cathode.[33,34] The reduction of Li ion diffusion coefficient is given by an empirical equation which is similar to others in the literature.[35,36] That is, the effective diffusion coefficient in the solid phase is given by:

$$D_S=D_{S,0}\left[1-\left(\frac{\varepsilon_{1,pos}^0-\varepsilon_{1,pos}}{\varepsilon_{1,pos}^0}\right)^{n_1}\right] \quad [30]$$

where $D_{S,0}$ is the initial solid phase diffusion coefficient, n_1 is an empirical factor which represents the effect of the formation of the film on the Li ion diffusion. n_1 can be obtained through experiments.

Boundary and initial conditions.— At the current collector/cathode interface ($x=0$):

The entire current density is carried by the solid phase, that is:

$$-\sigma_{eff}\left.\frac{\partial\phi_1}{\partial x}\right|_{x=0}=I_{app} \quad [31]$$

where I_{app} is the applied current density (the current divided by the projected electrode area), I_{app} is positive when charging the cell and is negative when discharging the cell.

For the same reason, the boundary condition for solution phase potential at $x=0$ is given by:

$$-\kappa_{eff}\left.\frac{\partial\phi_2}{\partial x}\right|_{x=0}=0 \quad [32]$$

The fluxes for the solution species are zero at $x=0$:

$$-D_{i,eff}\left.\frac{\partial c_i}{\partial x}\right|_{x=0}=0,\quad i=H_2O,Mn^{2+},H^+,Li^+ \quad [33]$$

At cathode/separator interface ($x=L_P$), the total current density is carried by the solution phase, therefore the solid phase current density is zero. The solution phase current density and the species flux on the left side of the interface should be equal to those on the right, therefore:

$$-\sigma_{eff}\left.\frac{\partial\phi_1}{\partial x}\right|_{x=L_P}=0 \quad [34]$$

$$i_2|_{x=L_p^-}=i_2|_{x=L_p^+} \quad [35]$$

$$-D_{\text{eff},pos}\left.\frac{\partial c_i}{\partial x}\right|_{x=L_p^-}=-D_{\text{eff},sep}\left.\frac{\partial c_i}{\partial x}\right|_{x=L_p^+},\quad i=H_2O,Mn^{2+},H^+,Li^+ \quad [36]$$

At the separator/Li metal interface ($x=L_P+L_S$), we set the potential at the Li metal electrode to be zero:

$$\phi_1|_{x=L_p+L_s}=0 \quad [37]$$

For the Li^+ ion, as the assumption above, the electric filed in the solution is not influence by H^+ and Mn^{2+}, therefore:

$$-D_{eff}\left.\frac{\partial c_{Li^+}}{\partial x}\right|_{x=L_p+L_s}=\frac{i_{b,Li}}{F}(1-t^+) \quad [38]$$

where,

$$i_{b,Li}=-k_{b,Li}c_{Li^+}^{0.5}\left[\exp\left(\frac{\alpha_aF}{RT}(-\phi_2)\right)-\exp\left(-\frac{\alpha_cF}{RT}(-\phi_2)\right)\right] \quad [39]$$

For H^+ and Mn^{2+}, it is assumed that when the cell is charged H^+ and Mn^{2+} are reduced at the anode surface as following reactions:

$$H^+ + e^- = H_2$$

$$Mn^{2+} + 2e^- = Mn$$

And, assuming for H^+ and Mn^{2+} there is no reduction/oxidation reactions when discharging cell,

$$-D_{eff}\left.\frac{\partial c_i}{\partial x}\right|_{x=L_p+L_s}=\frac{i_{b,i}}{F},\quad i=H^+,Mn^{2+} \quad [40]$$

where

$$i_{b,i}=k_{b,i}\left[-\exp\left(-\frac{\alpha_{c,i}F}{RT}(-\phi_2-U_i)\right)\right],\quad \text{Charge}$$
$$i_{b,i}=0,\quad \text{Discharge} \quad [41]$$

Table I. Electrode parameter values.

Parameter	Value	Parameter	Value
L_p	50 e-6 m	k_{Li}	1e-5 A m^{-2}
L_s	50 e-6 m	$k_{b,Li}$	6.1e-6 A m^{-2}
$\varepsilon_{2,pos}$	0.444	t_+	0.37
$\varepsilon_{2,sep}$	0.724	D_s	6e-15 m^2 s^{-1}
$\varepsilon^0{}_{1,pos}$	0.43	σ	10 S m^{-1}
R_{pos}	4.7 e-6 m	$\alpha_{a,Li}$	0.5
$Brugg_{pos}$	1.5	$\alpha_{c,Li}$	0.5
$Brugg_{sep}$	1.5	$c^0_{Li^+}$	2000 mol m^{-3}
R	8.314 J mol^{-1} K^{-1}	θ^0	0.3
F	96487 C $equiv^{-1}$	$c_{s,max}$	22040 mol m^{-3}
T	55°C	I_{app}	3.5 A m^{-2}
$\overline{V}$	4.1389e-5 m^3 mol^{-1}		

Table II. Parameter of side reactions.

Parameter	Value	Parameter	Value
U_{side}[a]	4.2 V	$c^0{}_{H2O}$[a]	4 mol m^{-3}
$a_{2,set}i_{0,s}$[a]	10.0 A m^{-3}*	$c^0{}_{H+}$[a]	4 mol m^{-3}
$\alpha_{a,s}$[a]	0.5	$c^0{}_{Mn2+}$[a]	0
k_2[b]	7.13e-10 m^6 mol^{-2} s^{-1}*	$k_{b,H+}$[a]	1.0e-18 A m mol^{-1}
k_3[a]	2.0e-10 m s^{-1}*	$k_{b,Mn2+}$[a]	1.0e-11 A m mol^{-1}
n_1[a]	0.12	α_{H+}[a]	0.01
$X_{c,set}$[a]	10%	α_{Mn2+}[a]	0.1
X_c[a]	10%*	$U^\theta_{H^+}$[a]	2.5 V
D_{H2O}[c]	3e-9 m^2 s^{-1}	$U^\theta_{Mn^{2+}}$[a]	1.5 V
D_{H+}[c]	5e-9 m^2 s^{-1}	D_{Mn2+}[c]	0.72e-9 m^2 s^{-1}

[a]Assumed.
[b]From Ref. 28.
[c]Referred to diffusion coefficients of ions at infinite dilution in water solvent.
*Except specification.

where $k_{b,i}$ is the reaction rate constant for species i on the Li metal surface, and

$$U_i = U_i^\theta + \frac{RT}{z_i F}\ln[\alpha_i c_i], \quad i = H^+, Mn^{2+} \qquad [42]$$

where U_i^θ is the equilibrium potential of the reaction on the Li metal surface for species i, α_i is the activity coefficient for species i in the solution.

The flux of H_2O is zero at the Li metal surface:

$$\left.\frac{\partial c_{H_2O}}{\partial x}\right|_{x=L_P+L_S} = 0 \qquad [43]$$

Current balance at $x = L_P + L_S$ is given by:

$$I_{app} = i_{b,Li} + i_{b,H^+} + i_{b,Mn^{2+}} \qquad [44]$$

The boundary conditions for the solid phase diffusion are given by:

$$-D_s\left.\frac{\partial c_s}{\partial r}\right|_{r=0} = 0 \qquad [45]$$

$$-D_s\left.\frac{\partial c_s}{\partial r}\right|_{r=R_{pos}} = \frac{i_{n,pos}}{F} \qquad [46]$$

The initial conditions used in the model are:

$$\begin{aligned} &c_i = c_i^0, \quad i = H_2O, Mn^{2+}, H^+, Li^+ \text{ at } 0 \le x \le L_P + L_S \\ &c_s = c_s^0, \text{ at } 0 \le r \le R_{pos} \text{ and } 0 \le x \le L_P + L_S \\ &\varepsilon_{j,pos} = \varepsilon^0_{j,pos},\ j = 1 \text{ at } 0 \le x \le L_P \end{aligned} \qquad [47]$$

An energy balance is not included in this model because all the simulations are at a low C-rate where the temperature across the cell does not change significantly.

Table I shows the values of the electrode parameters. Table II shows the values of the side reaction parameters. The open circuit potential of the spinel cathode and other model expressions are presented in Appendix.

Results and Discussion

The FORTRAN code was developed for the model and was solved using DARST (a DAE solver).[37] The model was used to investigate the effects of the cut off charge voltage, the carbon content in the cathode, the exchange current density of the solvent oxidation, and the reaction rate constants of the side reactions on the battery capacity fade.

Figure 1 shows the charge-discharge curves for selected cycle numbers (2, 25, and 50) of Li/LMO cell cycled at C/3 rate (1 C rate is 10.5 A m^{-2}) and 55°C between 3.5 and 4.5 V (vs Li/Li^+, all potentials below are relative to Li/Li^+ reference). As shown in Figure 1, the cell capacity decreases with repeated cycling. Also, the cell resistance increases slightly with the cycle number which is indicated in the voltages of the plateaus in different cycles. The simulation results are very similar to experimental values in which the voltages of the plateaus corresponding to lithium ion extraction/insertion do not change very much with cycling despite capacity loss.[3,12,38]

The capacity loss with cycle number is shown in Figure 2 (solid line). The cell capacity is reduced by 16% after 50 cycles at C/3 and 55°C between 3.5 and 4.5 V. For the same cycling conditions, the active material only decreases by 5% after 50 cycles as shown in the figure (dash line). Obviously, loss of active material amount cannot alone contribute to the overall capacity loss. Xia et al.[12] reported that the Li/LMO cell capacity decreases 19% after 50 cycles at C/3 and 50°C between 3.5 and 4.5 V, which is similar to the 16% reported by our model. Also, they measured that the capacity losses caused by Mn dissolution are only 34% and 23% of the overall capacity loss at 50°C and room temperature, respectively. In our model, about 30% of the total capacity loss is attributed to Mn dissolution which is close to the experimental values. However, in previous models the loss of active material due to Mn dissolution contributed significantly to the capacity losses.[18,20]

As shown in Figure 2 (the plot corresponding to the axes on the right), the Li ion diffusion coefficient is decreased from 3.5e-15 m^2 s^{-1}

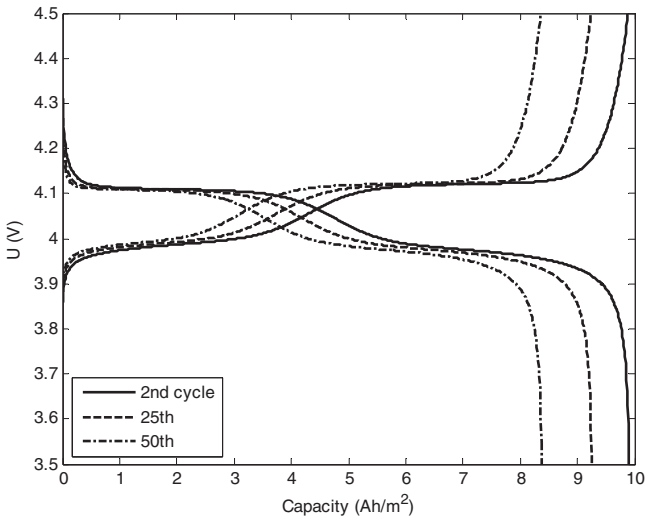

Figure 1. The 2nd, 25th, 50th charge and discharge curves of Li/LMO cell. The cell is cycled at C/3 rate and 55°C between 3.5 and 4.5 V.

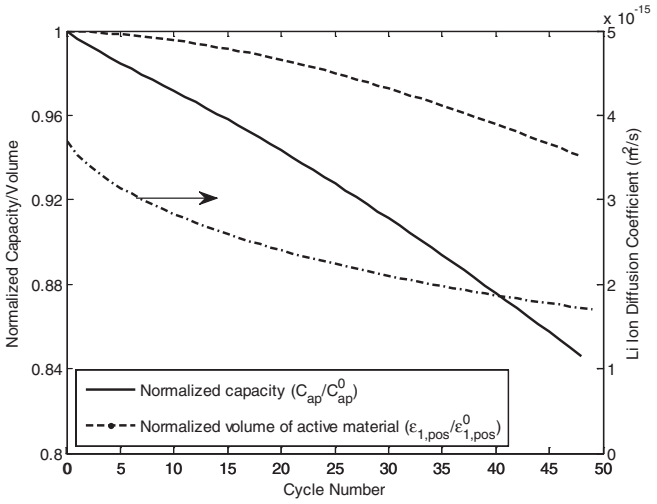

Figure 2. Normalized cell capacity, normalized volume fraction of active material and Li ion diffusion coefficient (the plot corresponding to the axes on the right) change with cycle number for Li/LMO cell. The cell was cycled at C/3 rate and 55°C between 3.5 and 4.5 V.

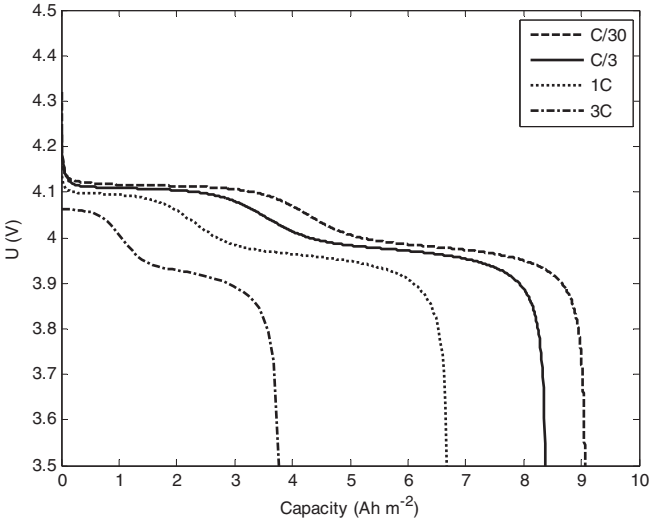

Figure 3. Discharge curves of aged Li/LMO cell at different current densities (C/30, C/3, 1C and 3 C) between 3.5 and 4.5 V at 55°C. Prior to each discharge, the cell has been cycled 50 times at C/3 and 55°C rate between 3.5 and 4.5 V from a fresh cell.

(diffusion coefficient recorded at the beginning of second cycle) to less than 2e-15 m^2 s^{-1} after 50 cycles. The decrease of Li ion diffusion coefficient is another critical factor that leads to the capacity loss. The decrease of Li ion diffusion coefficient would result in cell polarization loss. The electrochemically inactive material generated from the Mn dissolution reaction and the precipitation of the electrolyte decomposition products both can cause the inactive film growth on cathode. This film which is formed on the active material surface blocks Li ion transportation and decreases the effective solid phase diffusion coefficient. Those were reported in several experimental observations. Aurbach et al.[33] studied the impedance spectra of LMO cell polarized to 4.5 V with different time. The resistance of Li ion migration in the surface films was observed to increase from 171.9 Ω to 518.8 Ω after 120 min. This increase means that the kinetics of the electrode becomes sluggish. Zhang et al.[39] measured the Li ion diffusion coefficient as a function of cycle number for spinel LMO through an analysis of the Warburg impedance. The Li ion diffusion coefficient was found to decrease from 9.65e-10 cm^2 s^{-1} to 5.78e-10 cm^2 s^{-1} after 100 galvanostatic cycles with cutoff voltages of 3.4 V and 4.4 V. Das el al.[40] investigated the kinetics of Li ion diffusion in LMO thin film electrode by cyclic voltammetry as well as potential step chronoamperometry measurements. After repeated charge/discharge cycling, the Li ion diffusion coefficient was found to drop by almost one order of magnitude as compared to the original electrode. They reported that a surface electrolyte interface layer was formed on the electrode and this passive layer reduced the Li ion diffusion coefficient and lead to the observed capacity fading.

Figure 3 presents the rate dependent discharge curves of aged electrodes which have been cycled 50 times at C/3 rate and 55°C between 3.5 and 4.5 V from a fresh cell. When the current density applied to the aged electrode reduces from C/3 to C/30, about half of the loss discharge capacity can be recovered again. This confirms that the loss of active material is not the only factor causing capacity fading, but the cell polarization is another important contribution. Kim et al.[17] observed the charge capacity of aged LMO electrode increase with a decrease in the current density, which had been stored in the electrolyte 14 days at 60°C. The capacity was about 20 mAh g^{-1} at 50 mA g^{-1}, but 75 mAh g^{-1} at 2 mA g^{-1}. The capacity measured at the lower rate (2 mA g^{-1}) is not much smaller than that (108 mA g^{-1}) obtained from the fresh cell at the same rate. They revealed that during high-temperature storage, the electrolyte decomposition products were deposited on the LMO surface. The depiction layer was highly resistive for electron and Li^+ ion conduction and lead to a cell polarization and capacity loss.

The end of charge voltage (EOCV) is also a major factor in the battery cycle life. Figure 4 shows the variation of the cell capacity for 50 cycles with different cutoff charge voltages, namely 4.2, 4.3 and 4.5 V. Overcharging the cell to 4.5 V, the capacity fade is much more serious than that for the cells charged to 4.3 V as shown in the figure. In our model, the equilibrium potential of the solvent oxidation U_{side} is set to 4.2 V. Therefore, when the cell potential is above the U_{side}, the solvent decomposition increases much faster. Also, more acid is generated. This overcharging damage has been reported in the literatures.[12,33,41] Aurbach et al.[33] observed that there was more Mn dissolution from the LMO electrode which was charged to 4.5 V compared to the electrode charged to 4.2 V. Also, the electrode cycled in the potential range of 3.8–4.5 V at high rates, the dissolution was much less than that for the electrode cycled at low rated in the same voltage region. They revealed that the Mn dissolution process related to an oxidation of the solution. Xia et al.[12] reported that the capacity decreased 19.2% for Li/LMO cell cycled between 3.5 and 4.5 V at C/3 and 50°C after 50 cycles compared to 6.9% capacity loss cycled

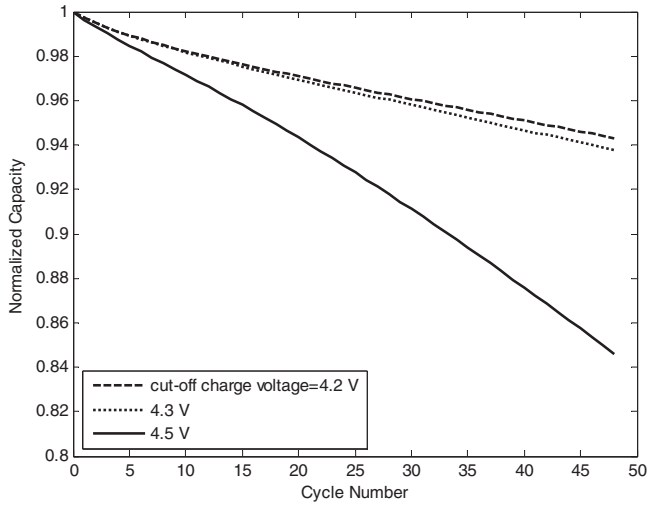

Figure 4. Normalized capacities as functions of cycle number for different end of charge voltages (4.2, 4.3 and 4.5 V). The Li/LMO cell is cycled at C/3 rate and 55°C, and the end of discharge voltage is 3.5 V.

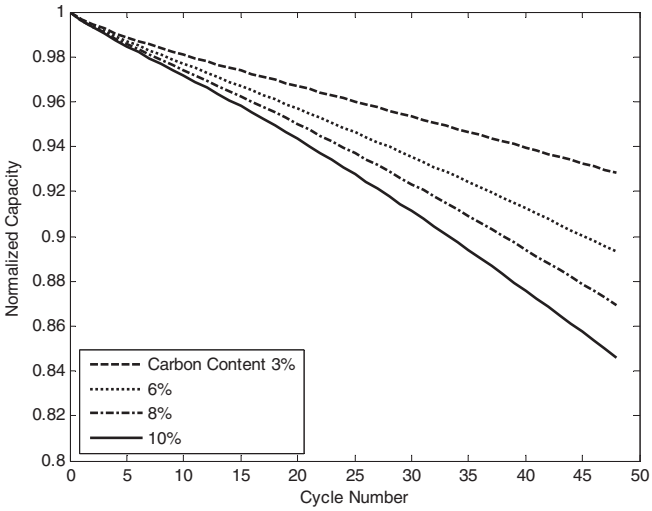

Figure 5. Normalized capacities as functions of cycle number for different carbon contents (3%, 6%, 8%, 10%, weight percent) in composite electrode. The Li/LMO cells are all cycled at C/3 and 55°C rate between 3.5 and 4.5 V.

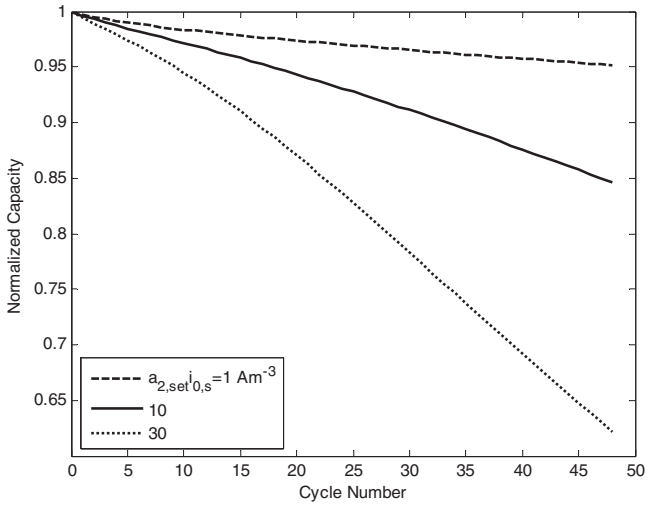

Figure 6. Normalized capacities as functions of cycle number for different solvent oxidation exchange current densities, $a_{2,set}i_{0,s}$, (1, 10, 30 A m^{-3}). The Li/LMO cells are all cycled at C/3 rate and 55°C between 3.5 and 4.5 V.

the cell between 3.5 and 4.23 V while other conditions remain the same. In our current model, the capacity loss after 50 cycles is about 16% cycled cell between 3.5 and 4.5 V at C/3 and 55°C. There is about 5% capacity loss when the cell is cycled between 3.5 and 4.3 V. Our simulation results are similar to the experimental data mentioned above.

In most of Li-ion cells, the carbon material has been used to improve electrical conductivity between the active particles in the cathode. The solvent oxidation currents were found to be roughly proportional to the surface area of the composite electrode. Since carbon used as conductor in the cathode has higher surface area compared to the active material, the surface area of the composite electrode is mainly dominated by that of carbon even though it is in a small quantity. In this model, the carbon content is related to cell performance by providing reaction sites for solvent oxidation through equation 19. Figure 5 shows the variation of capacity with different carbon contents in the composite cathode for the 50 cycles. As shown in figure, when the carbon content is decreased from 10% to 3%, the capacity loss is decreased from 16% to 6%. Also, the capacity loss after 50 cycles depends almost linearly on the carbon content. Guyomard et al.[21] determined that the variation of the irreversible capacity followed a straight line due to electrolyte oxidation at 55°C as a function of the carbon content (weight percent) in the composite electrode. Jang et al.[42] also reported that both the extent of solvent oxidation and the amount of Mn dissolution are proportional to carbon surface area. It should be mentioned that the effect of the carbon content on cell resistance is not considered in our current model. When carbon content is lower, the internal resistance increases much larger when the cell is aged. Consequently, the carbon content can be optimized by the tradeoff between the cell capacity loss and the polarization loss.

The adjustable parameters in the study mentioned above, such as the reaction rate constants (k_2, k_3) of side reactions were mainly fixed. For a better understanding of the contribution of different side reactions to the cell capacity fade, various parameters dominating the side reactions need to be investigated. The discussions shown below include the effects of the exchange current density of solvent oxidation, $i_{0,s}$, the reaction rate constant of $LiPF_6$ decomposition, k_2, and the reaction rate constant of LMO dissolution due to the acid attack, k_3, on the capacity fade of the Li/LMO half cells which are cycled between 3.5 and 4.5 V with current rate of C/3 at 55°C.

Figure 6 shows the effect of the exchange current density for the solvent oxidation reaction on the cell capacity fade. The stabilities of the solvent components (DME, EC, DMC, PC) in the cell are highly different. For example, ethers are easily oxidized whereas carbonates are relatively stable. Different compositions of the solvent species may lead to different values in $i_{0,s}$. The larger values $i_{0,s}$ mean that the electrolyte is less stable and the rate of the electrolyte oxidation increases during the cell cycling in the same voltage region. Consequently, the Mn dissolution and the capacity loss increase. As shown in Figure 6, the capacity loss is more than 5 times higher by changing $a_{2,set}i_{0,s}$ from 1 A m^{-3} to 30 A m^{-3}. A similar capacity loss tendency has been noted in many papers. For example, Jang et al.[4] observed that Li/LMO cells lost their capacity at faster rates in ethers and the capacity loss rate was slower in the carbonate-containing electrolytes. The Li/LMO cells in 1 M $LiClO_4$/PC/THF electrolyte lost half of its capacity after 50 cycles between 4.3 and 3.6 V. At the same cycling condition, the cells capacity in 1 M $LiClO_4$/PC/DEC only decreases about 10%. They explained that protons generated from solvent oxidation play an important role in Mn dissolution and ethers are relatively easier to be oxidized than carbonates. Therefore, the capacity loss in ethers is more significant compared to that in carbonates.

Water is undesirable for lithium ion batteries because it results in decompositions of the cell components, such as the electrolyte and the SEI film on the anode. However, there is often about ten of ppm water in the commercial electrolyte used in lithium ion cells. Moreover, many cathode materials are highly absorbent, and they draw a large amount of water into batteries. In addition water can be generated from a parasitic reaction (such as the side reaction shown in equation10) as discussed in Wang et al.[7] Figure 7 presents the effect of the reaction rate constant of the conductive salt decomposition, k_2, on the capacity fade at 55°C. The simulation results in Figure 7 show that an increase in the value of k_2 even by one order of magnitude dramatically accelerates the capacity loss which indicates that the variation of k_2 value has a significant influence on the cell capacity. That is, a high value of k_2 means that the rate of conductive salt decomposition with water will increase and more acid will be formed. That not only causes the resistance increase in the solution phase but also leads to more Mn dissolution. Therefore, a stable salt which has a small value of k_2 is more attractive than $LiFP_6$ for high temperature application. Likewise, water or acid scavenger additive such as zeolite would enhance cell performance, because they would absorb water or acid and reduce the apparent acid generation rate. Sano et al.[43] reported that substituting part of $LiPF_6$ in the electrolyte with $Li(C_2F_5SO_2)_2N$ (LiBETI) improved the LMO cell capacity retention when cycled at high temperature. LiBETI is not as facile as $LiPF_6$ to hydrolyze and produce acid. Therefore, it helps suppress acid formation from the hydrolysis. They also reported that phosphate additives improved the performance of LMO cells when cycled at high temperature.

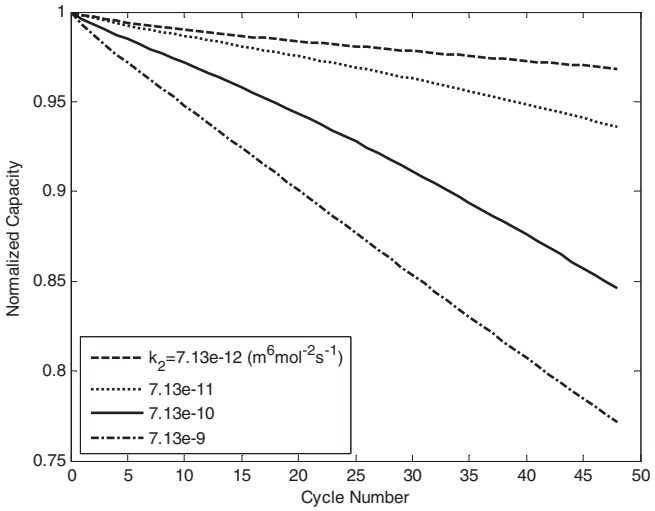

Figure 7. Normalized capacities as functions of cycle number for different $LiPF_6$ decomposition reaction rate constant, k_2, (7.13e-12, 7.13e-11, 7.13e-10, 7.13e-9 m^6 mol^{-2} s^{-1}). The Li/LMO cells are all cycled at C/3 rate and 55°C between 3.5 and 4.5 V.

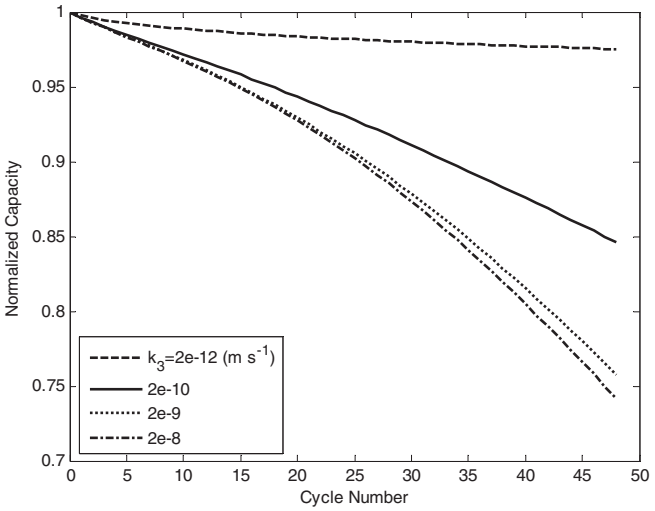

Figure 8. Normalized capacities as functions of cycle number for different reaction rate constants of LMO dissolution due to acid attack, k_3, (2e-12, 2e-10, 2e-9, 2e-8 m s^{-1}). The Li/LMO cells are all cycled at C/3 rate and 55°C between 3.5 and 4.5 V.

Figure 8 shows the influence of the reaction rate constant of LMO dissolution due to acid attack, k_3, on the cell capacity fading. By reducing k_3 from 2e-10 m s^{-1} to 2e-12 m s^{-1}, the capacity loss is reduced by 8 times (from 16% to 2%) for 50 cycles. This indicates that the stability of LMO in acid solution is very important for the cell performance operated at high temperature. When k_3 is changed from 2e-9 m s^{-1} to 2e-8 m s^{-1}, by contrast, the increase of the capacity loss is not significant. This indicates that Mn dissolution is controlled not only by the reaction rate constant but also by the acid supply. Coating and doping are effective ways to prevent the acid attacking on the LMO electrode. The stability of LMO in the acid solution increases and the value of k_3 becomes smaller. Wang et al.[7] reported that the Li_2CO_3 coated spinel LMO had better storage performance at elevated temperature than the original spinel. Deng et al.[44] observed that after Li-doped, the stability of spinel soaked in the solution at the elevated temperature increases, that is, the Mn dissolution from a Li-doped LMO sample decreases. At the same time, the cycling performance was improved significantly and the capacity retention ratio after 50 cycles at 60°C was improved to more than 90%.

Conclusions

A capacity fade model for a spinel based cathode was developed in this paper. The model considers the capacity loss due to the acid attack and the SEI film formation. The acid is generated from the decomposition of the solvent and the $LiPF_6$ solute, and then attacks the active material which leads to Mn dissolution and the formation of a SEI film on the cathode. The SEI film built on the cathode surface causes a decrease in the solid phase diffusion coefficient and causes the cell polarization loss. Case studies show that the end of charge voltage (EOCV) is a critical operation factor for capacity fading of the spinel based cathode. The effects of side reactions on cell performance are also investigated qualitatively. This study reveals that the stabilities of electrolyte and the spinel LMO are important for the cell life when the cell is cycled at the elevated temperature.

In this model, it was assumed that the Mn dissolution depends only on the concentration of acid species. This assumption may not represent the practical situation well. Consequently, a mechanism for the Mn dissolution at different states of charge will be implemented in a future model. A Carbon/LMO full cell model including the Mn^{2+} ion deposition on the carbon anode surface will also be included in a future model.

Appendix

Transport properties

The effective diffusion coefficient of species i in the electrolyte in region j, is determined by the following equation:

$$D_{eff,i} = D_i \varepsilon_{2,j}^{\text{brugg}_j}, \quad \begin{matrix} i = \text{H}_2\text{O}, \text{Mn}^{2+}, \text{H}^+, \text{Li}^+ \\ j = pos, sep \end{matrix} \qquad [A1]$$

where D_i denotes the diffusion coefficient of species i in the bulk electrolyte and brugg_j is the Bruggeman number of region j.The effective conductivity of Li^+ in the electrolyte in region j is as following:

$$\kappa_{\text{eff},j} = \kappa \varepsilon_{2,j}^{\text{brugg}_j}, \quad j = pos, sep \qquad [A2]$$

where κ is the conductivity of Li^+ in the bulk electrolyte.The effective conductivity of the solid phase is as following:

$$\sigma_{\text{eff}} = \sigma \varepsilon_{1,pos}^{\text{brugg}_j} \qquad [A3]$$

where σ is the conductivity of the solid phase.The concentration and temperature dependent Li^+ ionic conductivity, κ, and the diffusion coefficient,D_{Li^+}, in the electrolyte are given by:[45]

$$\kappa = 10^{-4} \times c_{Li^+} \left(\begin{matrix} -10.5 + 0.668 \times 10^{-3} c_{Li^+} + 0.494 \times 10^{-6} c_{Li^+}^2 + 0.074T \\ -1.78 \times 10^{-5} c_{Li^+} T - 8.86 \times 10^{-10} c_{Li^+}^2 T - 6.96 \times 10^{-5} T^2 + 2.80 \times 10^{-8} c_{Li^+} T^2 \end{matrix} \right)^2 \qquad [A4]$$

$$D_{Li^+} = 10^{-4} \times 10^{-4.43 - \frac{54}{T - 229 - 5.0 \times 10^{-3} c_{Li^+}} - 0.22 \times 10^{-3} c_{Li^+}} \qquad [A5]$$

Electrode Thermodynamic data

The open circuit potentials for the $LiMn_2O_4$ cathode as a function of state of charge is given by:[46]

$$U_p = 4.19829 + 0.0565661 \tanh(-14.5546\theta + 8.60942) - 0.0275479\left(\frac{1}{(0.998432-\theta)^{0.492465}} - 1.90111\right) - 0.157123\exp(-0.047380^8) + 0.810239\exp(-40(\theta - 0.133875)) \quad [A6]$$

where the SOC is defined by:

$$\theta = \frac{c_{s,surf}}{c_{s,\max}} \quad [A7]$$

List of Symbols

a	specific surface area, $m^2\ m^{-3}$
a_j	specific surface area in electrode region j, $m^2\ m^{-3}$
a_k	specific surface area for reaction k, $m^2\ m^{-3}$
a_2	specific surface area for solvent oxidation reaction, $m^2\ m^{-3}$
$a_{2,set}$	specific surface area preset for solvent oxidation reaction, $m^2\ m^{-3}$
brugg_j	Bruggeman coefficient of region j ($j = pos, sep$)
c_i	concentration for species i ($i = H_2O, Mn^{2+}, H^+, Li^+$), mol m^{-3}
c_i^0	initial concentration for species i ($i = H_2O, Mn^{2+}, H^+, Li^+$), mol m^{-3}
c_s	concentration of lithium ions in the solid particle, mol m^{-3}
c_s^0	initial concentration of lithium ions in the solid particle of electrode, mol m^{-3}
$c_{s,\max}$	maximum concentration of lithium ions in the solid particle, mol m^{-3}
D_i	electrolyte diffusion coefficient for species i ($i = H_2O, Mn^{2+}, H^+, Li^+$), $m^2\ s^{-1}$
D_s	lithium ion diffusion coefficient in the solid particle of electrode, $m^2\ s^{-1}$
F	Faraday's constant, 96487 C $equiv^{-1}$
I_{app}	applied current density, A m^{-2}
i_1	solid phase current density, A m^{-2}
i_2	solution phase current density, A m^{-2}
$i_{b,Li}$	current density on Li metal surface for Li ion, A m^{-2}
$i_{b,i}$	current density on Li metal surface for species i ($i = Mn^{2+}, H^+$), A m^{-2}
i_0	exchange current density, A m^{-2}
$i_{n,j}$	local transfer current density for Li ions intercalation/deintercalation reaction in electrode region j ($j = pos, sep$), A m^{-2}
i_s	local transfer current density for solvent oxidation reaction, A m^{-2}
k_i	reaction rate constant for side reaction i ($i = 2, 3$)
$k_{b,Li}$	reaction rate constant on Li metal surface for Li ion, A $m^{-0.5}$ $mol^{-0.5}$
$k_{b,i}$	reaction rate constant on Li metal surface for species i ($i = Mn^{2+}, H^+$), A m mol^{-1}
k_{Li}	Li intercalation/deintercalation reaction rate constant, A $m^{2.5}$ $mol^{-1.5}$
L_p	thickness of positive electrode, m
L_s	thickness of separator, m
n_1	adjust factor
pos	positive electrode
r	radial coordinate, m
R	universal gas constant, J mol^{-1} K^{-1}
$R_{s,i}$	reaction rate for side reaction i ($i = 1, 3$), mol m^{-2} s^{-1}
$R_{s,2}$	reaction rate for side reaction 2, mol m^{-3} s^{-1}
R_{pos}	radius of the active spinel, m
sep	separator
t_+	Li^+ transference number in the electrolyte
T	environment temperature, K
U_i	potential of reaction on the Li metal surface for species i ($i = Mn^{2+}, H^+$), V
U_i^θ	equilibrium potential of reaction on the Li metal surface for species i ($i = Mn^{2+}, H^+$), V
U_p	equilibrium potential of Li intercalation/deintercalation reaction in cathode, V
U_{side}	equilibrium potential of solvent oxidation side reaction, V
$\overline{V}$	molar volume of $LiMn_2O_4$
x	spatial coordinate, m
X_c	carbon content in the composite electrode,%
$X_{c,set}$	preset value of carbon content in the composite electrode, %
z_i	number of electrons for species i ($i = Mn^{2+}, H^+$)

Greek Letters

α_a	anodic transfer coefficient
α_c	cathodic transfer coefficient
α_i	the activity coefficient for species i ($i = Mn^{2+}, H^+$)
$\varepsilon_{1,pos}$	volume fraction of the solid phase in the positive electrode
$\varepsilon_{2,j}$	porosity of region j ($j = pos, sep$)
θ	dimensionless concentration of lithium ions in the solid particle ($\theta = c_{s,surf}/c_{s,\max}$)
θ^0	initial dimensionless concentration of lithium ions in the solid particle
κ	ionic conductivity of the electrolyte, S m^{-1}
κ_{eff}	effective ionic conductivity of the electrolyte, S m^{-1}
σ	electronic conductivity of the solid phase, S m^{-1}
σ_{eff}	effective electronic conductivity of the solid phase, S m^{-1}
ϕ_1	solid phase potential, V
ϕ_2	solution phase potential, V
η	overpotential, V
η_{Li}	overpotential for Li intercalation/deintercalation reaction, V
η_s	overpotential for the solvent oxidation side reaction, V

References

1. P. Arora, R. E. White, and M. Doyle, *J. Electrochem. Soc.*, **145**, 3647 (1998).
2. W. Choi and A. Manthiram, *J. Electrochem. Soc.*, **153**, A1760 (2006).
3. D. H. Jang, Y. J. Shin, and S. M. Oh, *J. Electrochem. Soc.*, **143**, 2204 (1996).
4. D. H. Jang and S. M. Oh, *J. Electrochem. Soc.*, **144**, 3342 (1997).
5. R. Chromik and F. Beck, *Electrochim. Acta*, **45**, 2175 (2000).
6. H. Lee, S. Kim, J. Jeon, and J. J. Cho, *J. Power Sources*, **173**, 972 (2007).
7. E. Wang, D. Ofer, W. Bowden, N. Iltchev, R. Moses, and K. Brandt, *J. Electrochem. Soc.*, **147**, 4023 (2000).
8. A. Du Pasquier, A. Blyr, P. Courjal, D. Larcher, G. Amatucci, B. Gerand, and J. M. Tarascon, *J. Electrochem. Soc.*, **146**, 428 (1999).
9. S. T. Myung, K. Hosoya, S. Komaba, H. Yashiro, Y. K. Sun, and N. Kumagai, *Electrochim. Acta*, **51**, 5912 (2006).
10. A. Antonini, C. Bellitto, M. Pasquali, and G. Pistoia, *J. Electrochem. Soc.*, **145**, 2726 (1998).
11. T. Numata, C. Amemiya, T. Kumeuchi, M. Shirakata, and M. Yonezawa, *J. Power Sources*, **97-8**, 358 (2001).
12. Y. Y. Xia, Y. H. Zhou, and M. Yoshio, *J. Electrochem. Soc.*, **144**, 2593 (1997).
13. S. Komaba, N. Kumagai, and Y. Kataoka, *Electrochim. Acta*, **47**, 1229 (2002).
14. H. Tsunekawa, S. Tanimoto, R. Marubayashi, M. Fujita, K. Kifune, and M. Sano, *J. Electrochem. Soc.*, **149**, A1326 (2002).
15. D. Aurbach, K. Gamolsky, B. Markovsky, G. Salitra, Y. Gofer, U. Heider, R. Oesten, and M. Schmidt, *J. Electrochem. Soc.*, **147**, 1322 (2000).
16. T. Eriksson, A. M. Andersson, A. G. Bishop, C. Gejke, T. Gustafsson, and J. O. Thomas, *J. Electrochem. Soc.*, **149**, A69 (2002).
17. D. Kim, S. Park, O. B. Chae, J. H. Ryu, Y. U. Kim, R. Z. Yin, and S. M. Oh, *J. Electrochem. Soc.*, **159**, A193 (2012).
18. J. Park, J. H. Seo, G. Plett, W. Lu, and A. M. Sastry, *Electrochem Solid St*, **14**, A14 (2011).
19. C. H. Lu and S. W. Lin, *Journal of Materials Research*, **17**, 1476 (2002).
20. L. Cai, Y. Dai, M. Nicolson, R. E. White, K. Jagannathan, and G. GBhatia, *J. Power Sources*, **221**, 191 (2013).
21. D. Guyomard and J. M. Tarascon, *J. Electrochem. Soc.*, **140**, 3071 (1993).
22. A. du Pasquier, A. Blyr, A. Cressent, C. Lenain, G. Amatucci, and J. M. Tarascon, *J Power Sources*, **81**, 54 (1999).
23. W. H. Kong, H. Li, X. J. Huang, and L. Q. Chen, *J. Power Sources*, **142**, 285 (2005).
24. R. Darling and J. Newman, *J. Electrochem. Soc.*, **145**, 990 (1998).

25. D. Aurbach, B. Markovsky, A. Shechter, Y. Ein-Eli, and H. Cohen, *J. Electrochem. Soc.*, **143**, 3809 (1996).
26. R. Oesten, U. Heider, and M. Schmidt, *Solid State Ionics*, **148**, 391 (2002).
27. C. G. Barlow, *Electrochem Solid St*, **2**, 362 (1999).
28. T. Kawamura, S. Okada, and J. Yamaki, *J. Power Sources*, **156**, 547 (2006).
29. R. Benedek and M. M. Thackeray, *Electrochem Solid St*, **9**, A265 (2006).
30. J. C. Hunter, *Journal of Solid State Chemistry*, **39**, 142 (1981).
31. H. Yamane, T. Inoue, M. Fujita, and M. Sano, *J. Power Sources*, **99**, 60 (2001).
32. D. Aurbach, B. Markovsky, A. Shechter, Y. EinEli, and H. Cohen, *J. Electrochem. Soc.*, **143**, 3809 (1996).
33. D. Aurbach, M. D. Levi, K. Gamulski, B. Markovsky, G. Salitra, E. Levi, U. Heider, L. Heider, and R. Oesten, *J. Power Sources*, **81**, 472 (1999).
34. K. Edstrom, T. Gustafsson, and J. O. Thomas, *Electrochim. Acta*, **50**, 397 (2004).
35. G. Sikha, B. N. Popov, and R. E. White, *J. Electrochem. Soc.*, **151**, A1104 (2004).
36. J. F. Yan, T. V. Nguyen, R. E. White, and R. B. Griffin, *J. Electrochem. Soc.*, **140**, 733 (1993).
37. K. E. Brenan, S. L. Campbell, and L. R. Petzold, *Numerical Solution of Initial Value Problems in Differential-Algebriac Equations*, Elsevier, New York, 1989.
38. Y. Y. Xia, T. Sakai, T. Fujieda, X. Q. Yang, X. Sun, Z. F. Ma, J. McBreen, and M. Yoshio, *J. Electrochem. Soc.*, **148**, A723 (2001).
39. D. Zhang, B. N. Popov, and R. E. White, *J. Power Sources*, **76**, 81 (1998).
40. S. R. Das, S. B. Majumder, and R. S. Katiyar, *J. Power Sources*, **139**, 261 (2005).
41. L. F. Wang, C. C. Ou, K. A. Striebel, and J. J. S. Chen, *J. Electrochem. Soc.*, **150**, A905 (2003).
42. D. H. Jang and S. M. Oh, *Electrochim. Acta*, **43**, 1023 (1998).
43. M. Sano, T. Hattori, T. Hibino, and M. Fujita, *Electrochem Solid St*, **10**, A270 (2007).
44. B. H. Deng, H. Nakamura, and M. Yoshio, *J. Power Sources*, **180**, 864 (2008).
45. L. O. Valoen and J. N. Reimers, *J. Electrochem. Soc.*, **152**, A882 (2005).
46. M. Doyle, J. Newman, A. S. Gozdz, C. N. Schmutz, and J. M. Tarascon, *J. Electrochem. Soc.*, **143**, 1890 (1996).